

Observation and study of $J/\psi \rightarrow \phi\eta\eta'$ at BESIII

M. Ablikim¹, M. N. Achasov^{10,d}, S. Ahmed¹⁵, M. Albrecht⁴, M. Alekseev^{56A,56C}, A. Amoroso^{56A,56C}, F. F. An¹, Q. An^{53,43}, J. Z. Bai¹, Y. Bai⁴², O. Bakina²⁷, R. Baldini Ferroli^{23A}, Y. Ban³⁵, K. Begzsuren²⁵, D. W. Bennett²², J. V. Bennett⁵, N. Berger²⁶, M. Bertani^{23A}, D. Bettoni^{24A}, F. Bianchi^{56A,56C}, E. Boger^{27,b}, I. Boyko²⁷, R. A. Briere⁵, H. Cai⁵⁸, X. Cai^{1,43}, O. Cakir^{46A}, A. Calcaterra^{23A}, G. F. Cao^{1,47}, S. A. Cetin^{46B}, J. Chai^{56C}, J. F. Chang^{1,43}, G. Chelkov^{27,b,c}, G. Chen¹, H. S. Chen^{1,47}, J. C. Chen¹, M. L. Chen^{1,43}, P. L. Chen⁵⁴, S. J. Chen³³, X. R. Chen³⁰, Y. B. Chen^{1,43}, W. Cheng^{56C}, X. K. Chu³⁵, G. Cibinetto^{24A}, F. Cossio^{56C}, H. L. Dai^{1,43}, J. P. Dai^{38,h}, A. Dbeyssi¹⁵, D. Dedovich²⁷, Z. Y. Deng¹, A. Denig²⁶, I. Denysenko²⁷, M. Destefanis^{56A,56C}, F. De Mori^{56A,56C}, Y. Ding³¹, C. Dong³⁴, J. Dong^{1,43}, L. Y. Dong^{1,47}, M. Y. Dong^{1,43,47}, Z. L. Dou³³, S. X. Du⁶¹, P. F. Duan¹, J. Fang^{1,43}, S. S. Fang^{1,47}, Y. Fang¹, R. Farinelli^{24A,24B}, L. Fava^{56B,56C}, S. Fegan²⁶, F. Feldbauer⁴, G. Felici^{23A}, C. Q. Feng^{53,43}, E. Fioravanti^{24A}, M. Fritsch⁴, C. D. Fu¹, Q. Gao¹, X. L. Gao^{53,43}, Y. Gao⁴⁵, Y. G. Gao⁶, Z. Gao^{53,43}, B. Garillon²⁶, I. Garzia^{24A}, A. Gilman⁵⁰, K. Goetzen¹¹, L. Gong³⁴, W. X. Gong^{1,43}, W. Gradl²⁶, M. Greco^{56A,56C}, M. H. Gu^{1,43}, Y. T. Gu¹³, A. Q. Guo¹, R. P. Guo^{1,47}, Y. P. Guo²⁶, A. Guskov²⁷, Z. Haddadi²⁹, S. Han⁵⁸, X. Q. Hao¹⁶, F. A. Harris⁴⁸, K. L. He^{1,47}, X. Q. He⁵², F. H. Heinsius⁴, T. Held⁴, Y. K. Heng^{1,43,47}, Z. L. Hou¹, H. M. Hu^{1,47}, J. F. Hu^{38,h}, T. Hu^{1,43,47}, Y. Hu¹, G. S. Huang^{53,43}, J. S. Huang¹⁶, X. T. Huang³⁷, X. Z. Huang³³, Z. L. Huang³¹, T. Hussain⁵⁵, W. Ikegami Andersson⁵⁷, M. Irshad^{53,43}, Q. Ji¹, Q. P. Ji¹⁶, X. B. Ji^{1,47}, X. L. Ji^{1,43}, X. S. Jiang^{1,43,47}, X. Y. Jiang³⁴, J. B. Jiao³⁷, Z. Jiao¹⁸, D. P. Jin^{1,43,47}, S. Jin^{1,47}, Y. Jin⁴⁹, T. Johansson⁵⁷, A. Julin⁵⁰, N. Kalantar-Nayestanaki²⁹, X. S. Kang³⁴, M. Kavatsyuk²⁹, B. C. Ke¹, I. K. Keshk⁴, T. Khan^{53,43}, A. Khoukaz⁵¹, P. Kiese²⁶, R. Kiuchi¹, R. Kliemt¹¹, L. Koch²⁸, O. B. Kolcu^{46B,f}, B. Kopf⁴, M. Kornicer⁴⁸, M. Kuemmel⁴, M. Kuessner⁴, A. Kupsc⁵⁷, M. Kurth¹, W. Kühn²⁸, J. S. Lange²⁸, P. Larin¹⁵, L. Lavezzi^{56C}, H. Leithoff²⁶, C. Li⁵⁷, Cheng Li^{53,43}, D. M. Li⁶¹, F. Li^{1,43}, F. Y. Li³⁵, G. Li¹, H. B. Li^{1,47}, H. J. Li^{1,47}, J. C. Li¹, J. W. Li⁴¹, Jin Li³⁶, K. J. Li⁴⁴, Kang Li¹⁴, Ke Li¹, Lei Li³, P. L. Li^{53,43}, P. R. Li^{47,7}, Q. Y. Li³⁷, W. D. Li^{1,47}, W. G. Li¹, X. L. Li³⁷, X. N. Li^{1,43}, X. Q. Li³⁴, Z. B. Li⁴⁴, H. Liang^{53,43}, Y. F. Liang⁴⁰, Y. T. Liang²⁸, G. R. Liao¹², L. Z. Liao^{1,47}, J. Libby²¹, C. X. Lin⁴⁴, D. X. Lin¹⁵, B. Liu^{38,h}, B. J. Liu¹, C. X. Liu¹, D. Liu^{53,43}, D. Y. Liu^{38,h}, F. H. Liu³⁹, Fang Liu¹, Feng Liu⁶, H. B. Liu¹³, H. L. Liu⁴², H. M. Liu^{1,47}, Huanhuan Liu¹, Huihui Liu¹⁷, J. B. Liu^{53,43}, J. Y. Liu^{1,47}, K. Liu⁴⁵, K. Y. Liu³¹, Ke Liu⁶, L. D. Liu³⁵, Q. Liu⁴⁷, S. B. Liu^{53,43}, X. Liu³⁰, Y. B. Liu³⁴, Z. A. Liu^{1,43,47}, Zhiqing Liu²⁶, Y. F. Long³⁵, X. C. Lou^{1,43,47}, H. J. Lu¹⁸, J. G. Lu^{1,43}, Y. Lu¹, Y. P. Lu^{1,43}, C. L. Luo³², M. X. Luo⁶⁰, T. Luo^{9,j}, X. L. Luo^{1,43}, S. Lusso^{56C}, X. R. Lyu⁴⁷, F. C. Ma³¹, H. L. Ma¹, L. L. Ma³⁷, M. M. Ma^{1,47}, Q. M. Ma¹, T. Ma¹, X. N. Ma³⁴, X. Y. Ma^{1,43}, Y. M. Ma³⁷, F. E. Maas¹⁵, M. Maggiora^{56A,56C}, S. Maldaner²⁶, Q. A. Malik⁵⁵, A. Mangoni^{23B}, Y. J. Mao³⁵, Z. P. Mao¹, S. Marcelllo^{56A,56C}, Z. X. Meng⁴⁹, J. G. Messchendorp²⁹, G. Mezzadri^{24B}, J. Min^{1,43}, R. E. Mitchell²², X. H. Mo^{1,43,47}, Y. J. Mo⁶, C. Morales Morales¹⁵, N. Yu. Muchnoi^{10,d}, H. Muramatsu⁵⁰, A. Mustafa⁴, Y. Nefedov²⁷, F. Nerling¹¹, I. B. Nikolaev^{10,d}, Z. Ning^{1,43}, S. Nisar⁸, S. L. Niu^{1,43}, X. Y. Niu^{1,47}, S. L. Olsen^{36,k}, Q. Ouyang^{1,43,47}, S. Pacetti^{23B}, Y. Pan^{53,43}, M. Papenbrock⁵⁷, P. Patteri^{23A}, M. Pelizaeus⁴, J. Pellegrino^{56A,56C}, H. P. Peng^{53,43}, Z. Y. Peng¹³, K. Peters^{11,g}, J. Pettersson⁵⁷, J. L. Ping³², R. G. Ping^{1,47}, A. Pitka⁴, R. Poling⁵⁰, V. Prasad^{53,43}, H. R. Qi², M. Qi³³, T. Y. Qi², S. Qian^{1,43}, C. F. Qiao⁴⁷, N. Qin⁵⁸, X. S. Qin⁴, Z. H. Qin^{1,43}, J. F. Qiu¹, S. Q. Qu³⁴, K. H. Rashid^{55,i}, C. F. Redmer²⁶, M. Richter⁴, M. Ripka²⁶, A. Rivetti^{56C}, M. Rolo^{56C}, G. Rong^{1,47}, Ch. Rosner¹⁵, A. Sarantsev^{27,e}, M. Savrié^{24B}, K. Schoenning⁵⁷, W. Shan¹⁹, X. Y. Shan^{53,43}, M. Shao^{53,43}, C. P. Shen², P. X. Shen³⁴, X. Y. Shen^{1,47}, H. Y. Sheng¹, X. Shi^{1,43}, J. J. Song³⁷, W. M. Song³⁷, X. Y. Song¹, S. Sosio^{56A,56C}, C. Sowa⁴, S. Spataro^{56A,56C}, G. X. Sun¹, J. F. Sun¹⁶, L. Sun⁵⁸, S. S. Sun^{1,47}, X. H. Sun¹, Y. J. Sun^{53,43}, Y. K. Sun^{53,43}, Y. Z. Sun¹, Z. J. Sun^{1,43}, Z. T. Sun²², Y. T. Tan^{53,43}, C. J. Tang⁴⁰, G. Y. Tang¹, X. Tang¹, I. Tapan^{46C}, M. Tiemens²⁹, B. Tsednee²⁵, I. Uman^{46D}, B. Wang¹, B. L. Wang⁴⁷, D. Wang³⁵, D. Y. Wang³⁵, Dan Wang⁴⁷, K. Wang^{1,43}, L. L. Wang¹, L. S. Wang¹, M. Wang³⁷, Meng Wang^{1,47}, P. Wang¹, P. L. Wang¹, W. P. Wang^{53,43}, X. F. Wang⁴⁵, X. L. Wang^{9,j}, Y. Wang^{53,43}, Y. F. Wang^{1,43,47}, Z. Wang^{1,43}, Z. G. Wang^{1,43}, Z. Y. Wang¹, Zongyuan Wang^{1,47}, T. Weber⁴, D. H. Wei¹², P. Weidenkaff²⁶, S. P. Wen¹, U. Wiedner⁴, M. Wolke⁵⁷, L. H. Wu¹, L. J. Wu^{1,47}, Z. Wu^{1,43}, L. Xia^{53,43}, Y. Xia²⁰, D. Xiao¹, Y. J. Xiao^{1,47}, Z. J. Xiao³², Y. G. Xie^{1,43}, Y. H. Xie⁶, X. A. Xiong^{1,47}, Q. L. Xiu^{1,43}, G. F. Xu¹, J. J. Xu^{1,47}, L. Xu¹, Q. J. Xu¹⁴, Q. N. Xu⁴⁷, X. P. Xu⁴¹, F. Yan⁵⁴, L. Yan^{56A,56C}, W. B. Yan^{53,43}, W. C. Yan², Y. H. Yan²⁰, H. J. Yang^{38,h}, H. X. Yang¹, L. Yang⁵⁸, R. X. Yang^{53,43}, Y. H. Yang³³, Y. X. Yang¹², Yifan Yang^{1,47}, Z. Q. Yang²⁰, M. Ye^{1,43}, M. H. Ye⁷, J. H. Yin¹, Z. Y. You⁴⁴, B. X. Yu^{1,43,47}, C. X. Yu³⁴, J. S. Yu²⁰, J. S. Yu³⁰, C. Z. Yuan^{1,47}, Y. Yuan¹, A. Yuncu^{46B,a}, A. A. Zafar⁵⁵, Y. Zeng²⁰, B. X. Zhang¹, B. Y. Zhang^{1,43}, C. C. Zhang¹, D. H. Zhang¹, H. H. Zhang⁴⁴, H. Y. Zhang^{1,43}, J. Zhang^{1,47}, J. L. Zhang⁵⁹, J. Q. Zhang⁴, J. W. Zhang^{1,43,47}, J. Y. Zhang¹, J. Z. Zhang^{1,47}, K. Zhang^{1,47}, L. Zhang⁴⁵, T. J. Zhang^{38,h}, X. Y. Zhang³⁷, Y. Zhang^{53,43}, Y. H. Zhang^{1,43}, Y. T. Zhang^{53,43}, Yang Zhang¹, Yao Zhang¹, Yi Zhang^{9,j}, Yu Zhang⁴⁷, Z. H. Zhang⁶, Z. P. Zhang⁵³, Z. Y. Zhang⁵⁸, G. Zhao¹, J. W. Zhao^{1,43}, J. Y. Zhao^{1,47}, J. Z. Zhao^{1,43}, Lei Zhao^{53,43}, Ling Zhao¹, M. G. Zhao³⁴, Q. Zhao¹, S. J. Zhao⁶¹, T. C. Zhao¹, Y. B. Zhao^{1,43}, Z. G. Zhao^{53,43}, A. Zhemchugov^{27,b}, B. Zheng⁵⁴, J. P. Zheng^{1,43}, Y. H. Zheng⁴⁷, B. Zhong³², L. Zhou^{1,43}, Q. Zhou^{1,47}, X. Zhou⁵⁸, X. K. Zhou^{53,43}, X. R. Zhou^{53,43}, X. Y. Zhou¹, Xiaoyu Zhou²⁰, Xu Zhou²⁰, A. N. Zhu^{1,47}, J. Zhu³⁴, J. Zhu⁴⁴, K. Zhu¹, K. J. Zhu^{1,43,47}, S. Zhu¹, S. H. Zhu⁵², X. L. Zhu⁴⁵, Y. C. Zhu^{53,43}, Y. S. Zhu^{1,47}, Z. A. Zhu^{1,47}, J. Zhuang^{1,43}, B. S. Zou¹, J. H. Zou¹

(BESIII Collaboration)

¹ Institute of High Energy Physics, Beijing 100049, People's Republic of China

² Beihang University, Beijing 100191, People's Republic of China

³ Beijing Institute of Petrochemical Technology, Beijing 102617, People's Republic of China

⁴ Bochum Ruhr-University, D-44780 Bochum, Germany

⁵ Carnegie Mellon University, Pittsburgh, Pennsylvania 15213, USA

- ⁶ Central China Normal University, Wuhan 430079, People's Republic of China
- ⁷ China Center of Advanced Science and Technology, Beijing 100190, People's Republic of China
- ⁸ COMSATS Institute of Information Technology, Lahore, Defence Road, Off Raiwind Road, 54000 Lahore, Pakistan
- ⁹ Fudan University, Shanghai 200443, People's Republic of China
- ¹⁰ G.I. Budker Institute of Nuclear Physics SB RAS (BINP), Novosibirsk 630090, Russia
- ¹¹ GSI Helmholtzcentre for Heavy Ion Research GmbH, D-64291 Darmstadt, Germany
- ¹² Guangxi Normal University, Guilin 541004, People's Republic of China
- ¹³ Guangxi University, Nanning 530004, People's Republic of China
- ¹⁴ Hangzhou Normal University, Hangzhou 310036, People's Republic of China
- ¹⁵ Helmholtz Institute Mainz, Johann-Joachim-Becher-Weg 45, D-55099 Mainz, Germany
- ¹⁶ Henan Normal University, Xinxiang 453007, People's Republic of China
- ¹⁷ Henan University of Science and Technology, Luoyang 471003, People's Republic of China
- ¹⁸ Huangshan College, Huangshan 245000, People's Republic of China
- ¹⁹ Hunan Normal University, Changsha 410081, People's Republic of China
- ²⁰ Human University, Changsha 410082, People's Republic of China
- ²¹ Indian Institute of Technology Madras, Chennai 600036, India
- ²² Indiana University, Bloomington, Indiana 47405, USA
- ²³ (A)INFN Laboratori Nazionali di Frascati, I-00044, Frascati, Italy; (B)INFN and University of Perugia, I-06100, Perugia, Italy
- ²⁴ (A)INFN Sezione di Ferrara, I-44122, Ferrara, Italy; (B)University of Ferrara, I-44122, Ferrara, Italy
- ²⁵ Institute of Physics and Technology, Peace Ave. 54B, Ulaanbaatar 13330, Mongolia
- ²⁶ Johannes Gutenberg University of Mainz, Johann-Joachim-Becher-Weg 45, D-55099 Mainz, Germany
- ²⁷ Joint Institute for Nuclear Research, 141980 Dubna, Moscow region, Russia
- ²⁸ Justus-Liebig-Universitaet Giessen, II. Physikalisches Institut, Heinrich-Buff-Ring 16, D-35392 Giessen, Germany
- ²⁹ KVI-CART, University of Groningen, NL-9747 AA Groningen, The Netherlands
- ³⁰ Lanzhou University, Lanzhou 730000, People's Republic of China
- ³¹ Liaoning University, Shenyang 110036, People's Republic of China
- ³² Nanjing Normal University, Nanjing 210023, People's Republic of China
- ³³ Nanjing University, Nanjing 210093, People's Republic of China
- ³⁴ Nankai University, Tianjin 300071, People's Republic of China
- ³⁵ Peking University, Beijing 100871, People's Republic of China
- ³⁶ Seoul National University, Seoul, 151-747 Korea
- ³⁷ Shandong University, Jinan 250100, People's Republic of China
- ³⁸ Shanghai Jiao Tong University, Shanghai 200240, People's Republic of China
- ³⁹ Shanxi University, Taiyuan 030006, People's Republic of China
- ⁴⁰ Sichuan University, Chengdu 610064, People's Republic of China
- ⁴¹ Soochow University, Suzhou 215006, People's Republic of China
- ⁴² Southeast University, Nanjing 211100, People's Republic of China
- ⁴³ State Key Laboratory of Particle Detection and Electronics, Beijing 100049, Hefei 230026, People's Republic of China
- ⁴⁴ Sun Yat-Sen University, Guangzhou 510275, People's Republic of China
- ⁴⁵ Tsinghua University, Beijing 100084, People's Republic of China
- ⁴⁶ (A)Ankara University, 06100 Tandogan, Ankara, Turkey; (B)Istanbul Bilgi University, 34060 Eyup, Istanbul, Turkey; (C)Uludag University, 16059 Bursa, Turkey; (D)Near East University, Nicosia, North Cyprus, Mersin 10, Turkey
- ⁴⁷ University of Chinese Academy of Sciences, Beijing 100049, People's Republic of China
- ⁴⁸ University of Hawaii, Honolulu, Hawaii 96822, USA
- ⁴⁹ University of Jinan, Jinan 250022, People's Republic of China
- ⁵⁰ University of Minnesota, Minneapolis, Minnesota 55455, USA
- ⁵¹ University of Muenster, Wilhelm-Klemm-Str. 9, 48149 Muenster, Germany
- ⁵² University of Science and Technology Liaoning, Anshan 114051, People's Republic of China
- ⁵³ University of Science and Technology of China, Hefei 230026, People's Republic of China
- ⁵⁴ University of South China, Hengyang 421001, People's Republic of China
- ⁵⁵ University of the Punjab, Lahore-54590, Pakistan
- ⁵⁶ (A)University of Turin, I-10125, Turin, Italy; (B)University of Eastern Piedmont, I-15121, Alessandria, Italy; (C)INFN, I-10125, Turin, Italy
- ⁵⁷ Uppsala University, Box 516, SE-75120 Uppsala, Sweden
- ⁵⁸ Wuhan University, Wuhan 430072, People's Republic of China
- ⁵⁹ Xinyang Normal University, Xinyang 464000, People's Republic of China
- ⁶⁰ Zhejiang University, Hangzhou 310027, People's Republic of China
- ⁶¹ Zhengzhou University, Zhengzhou 450001, People's Republic of China

^a Also at Bogazici University, 34342 Istanbul, Turkey

^b Also at the Moscow Institute of Physics and Technology, Moscow 141700, Russia

^c Also at the Functional Electronics Laboratory, Tomsk State University, Tomsk, 634050, Russia

^d Also at the Novosibirsk State University, Novosibirsk, 630090, Russia

^e Also at the NRC "Kurchatov Institute", PNPI, 188300, Gatchina, Russia

^f Also at Istanbul Arel University, 34295 Istanbul, Turkey

^g Also at Goethe University Frankfurt, 60323 Frankfurt am Main, Germany

^h Also at Key Laboratory for Particle Physics, Astrophysics and Cosmology, Ministry of Education; Shanghai Key Laboratory for Particle Physics and Cosmology; Institute of Nuclear and Particle Physics, Shanghai 200240, People's Republic of China

ⁱ Government College Women University, Sialkot - 51310. Punjab, Pakistan.

^j Key Laboratory of Nuclear Physics and Ion-beam Application (MOE) and Institute of Modern Physics, Fudan University, Shanghai 200443, People's Republic of China

^k Currently at: Center for Underground Physics, Institute for Basic Science, Daejeon 34126, Korea

We report the observation and study of $J/\psi \rightarrow \phi\eta\eta'$ decay using 1.3×10^9 J/ψ events collected with the BESIII detector. Its branching fraction including all the possible intermediate states is measured to be $(2.32 \pm 0.06 \pm 0.16) \times 10^{-4}$. A structure denoted as X is observed in the $\phi\eta'$ mass spectrum in 2.0–2.1 GeV/ c^2 region. A simultaneous fit to $\phi\eta'$ mass spectra with two decay modes of η' meson ($\gamma\pi^+\pi^-$ and $\eta\pi^+\pi^-$) is performed. Assuming the J^P value of the structure as 1^- , the significance of the structure is evaluated to be 5.3σ ; the mass and width are determined to be $(2002.1 \pm 27.5 \pm 15.0)$ MeV/ c^2 and $(129 \pm 17 \pm 7)$ MeV, respectively; the product branching fraction is measured to be $\mathcal{B}(J/\psi \rightarrow \eta X) \times \mathcal{B}(X \rightarrow \phi\eta') = (9.8 \pm 1.2 \pm 1.5) \times 10^{-5}$. Assuming the J^P value of the structure as 1^+ , the significance of the structure is evaluated to be 4.9σ ; the mass and width are determined to be $(2062.8 \pm 13.1 \pm 4.2)$ MeV/ c^2 and $(177 \pm 36 \pm 20)$ MeV, respectively; the product branching fraction is measured to be $\mathcal{B}(J/\psi \rightarrow \eta X) \times \mathcal{B}(X \rightarrow \phi\eta') = (9.6 \pm 1.4 \pm 1.6) \times 10^{-5}$. The angular distribution is studied and the two assumptions could hardly be distinguished due to the limited statistics. In all measurements the first uncertainties are statistical and the second systematic.

PACS numbers: 13.25.Gv, 13.66.Bc, 14.40.Rt

I. INTRODUCTION

The exotic hadrons, e.g., glueballs, hybrid states and multi-quark states, are allowed in the framework of the Quantum Chromodynamics (QCD), but no conclusive evidence has been found yet. The decay of $J/\psi \rightarrow VPP$, where V is a vector meson and P is a pseudoscalar meson, is an ideal environment to study the light hadron spectroscopy and to search for the new hadrons. There have been theoretical [1–4] and experimental [5–10] studies performed mainly focused on the V recoil system to search for the exotic hadrons. The P recoil system might also be utilized to search for the exotic hadrons. For example, the $Y(2175)$, denoted as $\phi(2170)$ by the Particle Data Group (PDG) [11], was confirmed in $J/\psi \rightarrow \eta Y(2175)$, $Y(2175) \rightarrow \phi f_0(980)$ decay by BESII [12] and BESIII [13]. Searching for its decay to $\phi\eta'$ state might provide valuable inputs for understanding its nature [14]. The decay of $J/\psi \rightarrow \phi\eta\eta'$ has not been studied before, and investigating this process can help to understand J/ψ decay mechanism and offers an opportunity to study possible intermediate states.

In this article, we report the observation and study of $J/\psi \rightarrow \phi\eta\eta'$ decay using $(1310.6 \pm 7.0) \times 10^6$ J/ψ events [15] collected with the BESIII detector. Its branching fraction including all the possible intermediate states is measured. A structure denoted as X is observed in the $\phi\eta'$ mass spectrum in 2.0–2.1 GeV/ c^2 region. The mass and width of the structure, as well as the branching fraction $\mathcal{B}(J/\psi \rightarrow \eta X) \times \mathcal{B}(X \rightarrow \phi\eta')$, are measured. The ϕ meson is reconstructed through its K^+K^- decay mode, η through $\gamma\gamma$, and η' through both $\gamma\pi^+\pi^-$ and $\eta\pi^+\pi^-$ (with the $\eta \rightarrow \gamma\gamma$), denoted as mode I and mode

II, respectively.

II. BESIII EXPERIMENT AND MONTE CARLO SIMULATION

The BESIII detector is a magnetic spectrometer [16] located at the Beijing Electron Position Collider (BEPIC) [17]. The cylindrical core of the BESIII detector consists of a helium-based multilayer drift chamber (MDC), a plastic scintillator time-of-flight system (TOF), and a CsI(Tl) electromagnetic calorimeter (EMC), which are all enclosed in a superconducting solenoidal magnet providing a 1.0 T (0.9 T in 2012) magnetic field. The solenoid is supported by an octagonal flux-return yoke with resistive plate counter muon identifier modules interleaved with steel. The acceptance of charged particles and photons is 93% over 4π solid angle. The charged-particle momentum resolution at 1 GeV/ c is 0.5%, and the dE/dx resolution is 6% for the electrons from Bhabha scattering. The EMC measures photon energies with a resolution of 2.5% (5%) at 1 GeV in the barrel (end cap) region. The time resolution of the TOF barrel part is 68 ps, while that of the end cap part is 110 ps.

Simulated samples produced with the GEANT4-based [18] Monte Carlo (MC) package which includes the geometric description of the BESIII detector and the detector response, are used to determine the detection efficiency and to estimate the backgrounds. The simulation includes the beam energy spread and initial state radiation (ISR) in the e^+e^- annihilations modelled with the generator KKMC [19]. The inclusive MC sample con-

sists of the production of the J/ψ resonance, and the continuum processes incorporated in KKMC [19]. The known decay modes are modelled with EVTGEN [20] using branching fractions taken from the PDG [11], and the remaining unknown decays from the charmonium states with LUNDCHARM [21]. The final state radiations (FSR) from charged final state particles are incorporated with the PHOTOS package [22].

III. EVENT SELECTION AND DATA ANALYSIS

Charged tracks are reconstructed from hits in the MDC. We select four charged tracks with net charge zero in the polar angle range $|\cos\theta| < 0.93$, and require their points of closest approach to the e^+e^- interaction point to be within ± 10 cm in the beam direction and 1 cm in the plane perpendicular to the beam direction. The dE/dx and TOF measurements are combined to form particle identification (PID) confidence levels for the π , K and p hypotheses. We require that one K^+K^- pair and one $\pi^+\pi^-$ pair are identified. A vertex fit that assumes the $\pi^+\pi^-K^+K^-$ tracks all come from a common vertex is applied.

Photons are reconstructed from electromagnetic showers in the EMC. At least three photons are required for mode I and four for mode II. The minimum energy for showers to be identified as photons in the barrel region ($|\cos\theta| < 0.8$) is 25 MeV, and in the end caps ($0.86 < |\cos\theta| < 0.92$) 50 MeV. Showers out of the above regions are poorly reconstructed and not used in this analysis. To suppress showers from charged particles, a photon must be separated by at least 10 degrees from the nearest charged track. EMC cluster timing requirements suppress electronic noise and energy deposits unrelated to this event.

Four-constraint (4C) kinematic fits are applied to all combinations of photons, and only the combination with the smallest χ_{4C}^2 is kept, and we only keep those events with $\chi_{4C}^2 \leq 40$ for mode I and $\chi_{4C}^2 \leq 80$ for mode II. To suppress background events containing π^0 's, those events with the invariant mass of any photon pair within a π^0 mass window ($0.12 \leq M(\gamma\gamma) \leq 0.15$ GeV/ c^2) are rejected. For mode I, the combination with the smallest value of $\delta_1^2 = [M(\gamma_1\gamma_2) - m_\eta]^2/\sigma_\eta^2 + [M(\gamma_3\pi^+\pi^-) - m_{\eta'}]^2/\sigma_{\eta'}^2$ is used to assign photons to the η and η' . Here m_η and $m_{\eta'}$ are the nominal η and η' masses [11], respectively; σ_η and $\sigma_{\eta'}$ are the mass resolutions determined from signal MC simulation. Mass windows for the η , ϕ and η' mesons are (in GeV/ c^2): $0.522 \leq M(\gamma\gamma) \leq 0.573$, $1.010 \leq M(K^+K^-) \leq 1.030$ and $0.936 \leq M(\gamma\pi^+\pi^-) \leq 0.979$. $M(\pi^+\pi^-)$ is required to be less than 0.87 GeV/ c^2 to suppress the background from the $J/\psi \rightarrow \eta\phi f_0(980)$ process as shown in Fig. 1. For mode II, we use the combination with the smallest $\delta_2^2 = [M(\gamma_1\gamma_2) - m_\eta]^2/\sigma_\eta^2 + [M(\gamma_3\gamma_4) - m_\eta]^2/\sigma_\eta^2$ for the best η meson combination; the η for which $M(\pi^+\pi^-\eta)$ is closest to $m_{\eta'}$ is at-

tributed to the candidate decaying from the η' . Mass windows for the η , ϕ and η' mesons are (in GeV/ c^2): $0.509 \leq M(\gamma\gamma) \leq 0.586$, $1.010 \leq M(K^+K^-) \leq 1.030$ and $0.920 \leq M(\eta\pi^+\pi^-) \leq 0.995$.

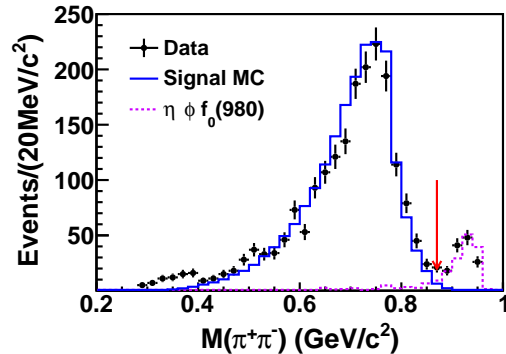


FIG. 1. Invariant mass spectrum of $\pi^+\pi^-$ for mode I, where the crosses are experimental data, the solid histogram shows the signal MC simulation, the dotted histogram shows the background from the $J/\psi \rightarrow \eta\phi f_0(980)$ process, and the arrow represents the mass requirement.

Figure 2 shows the distributions of $M(\gamma\pi^+\pi^-)$ versus $M(K^+K^-)$ for mode I and $M(\eta\pi^+\pi^-)$ versus $M(K^+K^-)$ for mode II. The background inferred from the η sidebands is negligible according to the study of data and inclusive J/ψ decays, and the non- ϕ and/or non- η' backgrounds are determined from the 2D sidebands of the ϕ and η' mesons, following the similar procedure in Ref. [23]. The ϕ and η' meson signals are clearly shown in both modes in the figure. The three body decay process of $J/\psi \rightarrow \phi\eta\eta'$ is thus established, which is the first observation of this decay.

IV. MEASUREMENT OF $\mathcal{B}(J/\psi \rightarrow \phi\eta\eta')$

The branching fraction of $J/\psi \rightarrow \phi\eta\eta'$ final state including all possible intermediate states is measured. Following the same procedure in Ref. [24], the regions of $M^2(\phi\eta')$ versus $M^2(\phi\eta)$ are divided into 40×40 areas (each area is tagged with i and j) and the numbers of data (n_{data}^{ij}), non- ϕ and/or non- η' background (n_{bkg}^{ij}) and efficiency (ϵ_{ij}) are obtained individually in each area. Then $\mathcal{B}(J/\psi \rightarrow \phi\eta\eta')$ is determined by

$$\mathcal{B} = \frac{N_{\text{corr}}}{N_{J/\psi} \mathcal{B}(\eta \rightarrow 2\gamma) \mathcal{B}(\phi \rightarrow K^+K^-) \mathcal{B}_{\eta'}}, \quad (1)$$

where N_{corr} is the signal number after efficiency correction and it is calculated by $N_{\text{corr}} = \sum_{ij} [(n_{\text{data}}^{ij} - n_{\text{bkg}}^{ij})/\epsilon_{ij}]$; $N_{J/\psi}$ [15] is the total number of J/ψ events; \mathcal{B} means the branching fractions from PDG [11], in which $\mathcal{B}_{\eta'}$ is $\mathcal{B}(\eta' \rightarrow \gamma\pi^+\pi^-)$ for mode I and $\mathcal{B}(\eta' \rightarrow \eta\pi^+\pi^-) \times \mathcal{B}(\eta \rightarrow \gamma\gamma)$ for mode II. $\mathcal{B}(J/\psi \rightarrow \phi\eta\eta')$ is determined to be $(2.31 \pm 0.07) \times 10^{-4}$ for mode I and $(2.34 \pm 0.12) \times 10^{-4}$

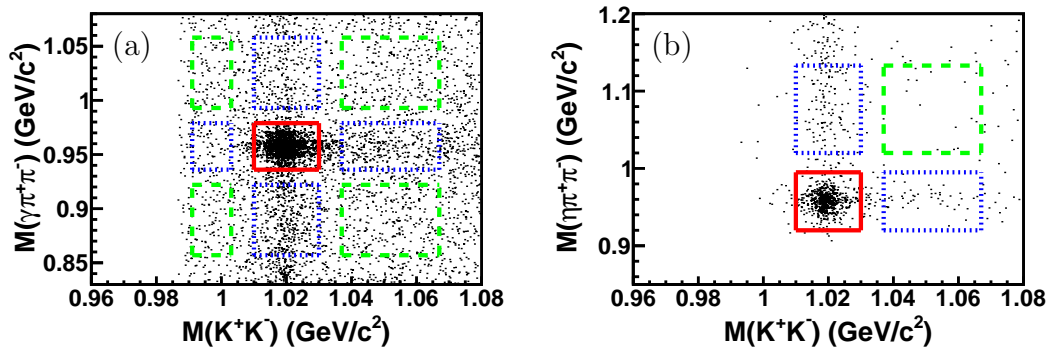


FIG. 2. Distributions of $M(\gamma\pi^+\pi^-)$ versus $M(K^+K^-)$ for mode I (a) and $M(\eta\pi^+\pi^-)$ versus $M(K^+K^-)$ for mode II (b), where the solid rectangles show the signal regions; the dotted and dashed rectangles represent the 2D sidebands.

for mode II, where the uncertainties are statistical only. The weighted average [25] of the results for the two η' decay modes is $(2.32 \pm 0.06 \pm 0.16) \times 10^{-4}$, after taking into account the correlations between the uncertainties from the two modes as denoted with asterisks in Table I.

The systematic uncertainties in $\mathcal{B}(J/\psi \rightarrow \phi\eta\eta')$ measurements are shown in Table I. The uncertainties from MDC tracking and PID efficiencies are established to be 1.0% per pion/kaon in Refs. [26, 27]. The uncertainty related to photon detection is determined to be 0.6% per photon in Ref. [28]. The uncertainties associated with the 4C kinematic fit are studied with the track parameter correction method [29] and the differences between the efficiencies with and without corrections are regarded as uncertainties; the influence of χ_{4C}^2 requirement is also considered in the uncertainty determination. The sideband regions of ϕ and η' mesons are varied by 1σ (the width of signal region corresponds to 3σ), and the effects on the branching fraction measurements are assigned as uncertainties. The uncertainties from mass windows are determined by smearing the mass spectra from phase space (PHSP) MC samples to compensate for the differences between the resolutions from data and MC simulation; the differences between efficiencies before and after smearing are taken as uncertainties. The influences of finite MC statistics are taken into account. The uncertainties due to quoted branching fractions and number of J/ψ events are from the PDG [11] and Ref. [15], respectively. The uncertainties from 2D binning are obtained by changing the numbers of areas in $\mathcal{B}(J/\psi \rightarrow \phi\eta\eta')$ determination. The total systematic uncertainties are obtained by summing all individual contributions in quadrature, assuming they are independent.

V. STUDY OF THE INTERMEDIATE STATE IN $\phi\eta'$ MASS SPECTRUM

Figure 3 shows the Dalitz plots for modes I and II, both of which have concentrations of events with

TABLE I. Systematic uncertainties in $\mathcal{B}(J/\psi \rightarrow \phi\eta\eta')$. The correlated sources between two η' decay modes are denoted with asterisks.

Sources	Mode I (%)	Mode II (%)
MDC tracking*	4.0	4.0
PID*	4.0	4.0
Photon detection*	1.8	2.4
Kinematic fit	2.5	1.1
Sideband regions	0.1	0.3
Mass window for η	0.5	0.7
Mass window for ϕ	0.9	1.0
Mass window for η'	0.7	0.6
MC statistics	0.6	0.9
Branching fractions*	2.1	2.1
Number of J/ψ *	0.6	0.6
2D binning	3.9	2.2
Total	8.0	7.2

$M^2(\phi\eta')$ values near $4.5 \text{ (GeV}/c^2)^2$. There are also diagonal bands in both modes corresponding to $J/\psi \rightarrow \phi f_0(1500), f_0(1500) \rightarrow \eta\eta'$ process based on MC study. Apart from these, no other structures are evident.

A. Simultaneous fit

With the assumption that there is an X structure in the $\phi\eta'$ mass spectrum in $2.0 - 2.1 \text{ GeV}/c^2$ region, corresponding to the clusters near $4.5 \text{ (GeV}/c^2)^2$ visible in Fig. 3, a simultaneous fit is performed on the $\phi\eta'$ mass spectra for modes I and II. Since the spin-parity value (J^P) of the structure could affect the relative orbital angular momenta between the decay products of $J/\psi \rightarrow \eta X$ and $X \rightarrow \phi\eta'$, the fits with two different assumptions on the J^P value are both performed. However, due to the limited statistics, they could hardly be distinguished. In the simultaneous fits, the interference between the structure and the direct decay of $J/\psi \rightarrow \phi\eta\eta'$ is not considered.

Assuming the J^P value of the structure as 1^- , the

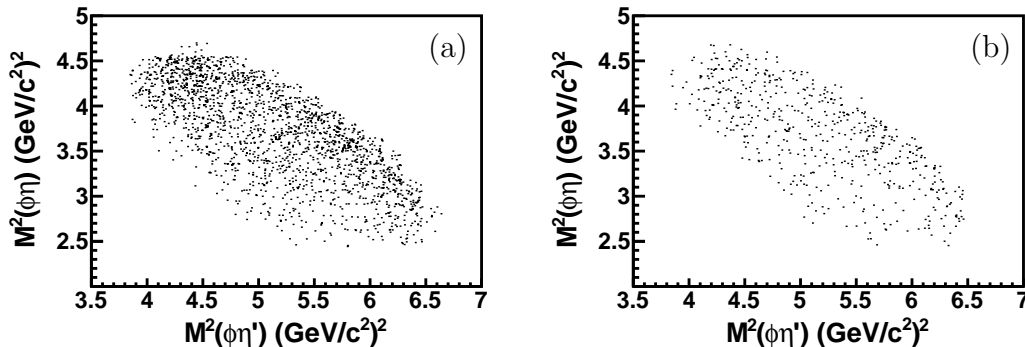


FIG. 3. Dalitz plots for modes I (a) and II (b).

signal component is parametrized by

$$\left(\frac{1}{m^2 - M^2 + iM\Gamma/c^2} \right)^2 \times (pq)^3 \times \epsilon \otimes R, \quad (2)$$

where m is the reconstructed mass of $\phi\eta'$ system; M and Γ are the mass and width of the structure in the constant-width relativistic Breit-Wigner (BW) function; the P-wave PHSP factor $(pq)^3$ is considered in the partial width, where p is the ϕ momentum in the $\phi\eta'$ rest frame, and q is the η momentum in the J/ψ rest frame; ϵ denotes the efficiency and R is the double-Gaussian resolution function, both of which are determined from signal MC simulation. The mass and width of the BW function are allowed to float but are constrained to be the same for both modes; the signal ratio of the two modes is fixed based on PDG η' branching fractions [11] and MC-determined efficiencies. The total signal yield of the two modes is allowed to float in the fit. The background components consist of non-resonant $\phi\eta\eta'$, $J/\psi \rightarrow \phi f_0(1500)$, $f_0(1500) \rightarrow \eta\eta'$ and non- ϕ and/or non- η' processes. For the non-resonant $\phi\eta\eta'$ process, the line shapes are derived from $J/\psi \rightarrow \phi\eta\eta'$ PHSP MC simulation, and the ratio of background numbers for the two modes is fixed, similar to the signal case. For $J/\psi \rightarrow \phi f_0(1500)$, $f_0(1500) \rightarrow \eta\eta'$ background, whose influence on the observation of the structure is small, the shapes are from MC simulation; $\mathcal{B}(J/\psi \rightarrow \phi f_0(1500)) \times \mathcal{B}(f_0(1500) \rightarrow \pi\pi)$ and $\mathcal{B}(J/\psi \rightarrow \phi f_0(1500)) \times \mathcal{B}(f_0(1500) \rightarrow K\bar{K})$ from BESII [9], together with $\mathcal{B}(f_0(1500) \rightarrow \pi\pi)$, $\mathcal{B}(f_0(1500) \rightarrow K\bar{K})$ and $\mathcal{B}(f_0(1500) \rightarrow \eta\eta')$ from PDG [11], are used to obtain the expected $f_0(1500)$ number in this analysis, and the background number is fixed to the expected value. The non- ϕ and/or non- η' backgrounds are determined from the 2D sidebands of the ϕ and η' mesons as shown in Fig. 2.

Figure 4 shows the results of the simultaneous fit, where the mass and width of the structure are determined to be (2002.1 ± 27.5) MeV/ c^2 and (129 ± 17) MeV, respectively. The log-likelihood value is 15591.8, with a goodness-of-fit value of $\chi^2/\text{d.o.f.}$ to be $20.98/26 = 0.81$ for mode I and $25.97/26 = 1.00$ for mode II. The statis-

tical significance of the new structure is calculated to be larger than 10σ , determined from the change of the log-likelihood values and the numbers of free parameters in the fits with and without the inclusion of the structure. After smearing the likelihood curve with the Gaussian-distributed systematic uncertainties (Table III), the significance is evaluated to be 5.3σ . Many checks are made to make sure that none of the possible background contributions could produce peaking backgrounds in $2.0 - 2.1$ GeV/ c^2 region in the $\phi\eta'$ mass spectrum. Comparison between data and MC also indicates no significant structures in the $\phi\eta$ mass spectrum.

Assuming the J^P value of the structure as 1^+ , the simultaneous fit with the S-wave PHSP factor pq in the partial width is performed as shown in Fig. 5. The mass and width of the structure are determined to be (2062.8 ± 13.1) MeV/ c^2 and (177 ± 36) MeV, respectively. The log-likelihood value is 15595.9, with a goodness-of-fit value of $\chi^2/\text{d.o.f.}$ to be $16.68/26 = 0.64$ for mode I and $24.36/26 = 0.94$ for mode II. The significance of the structure after considering the systematic uncertainties (Table IV) is evaluated to be 4.9σ .

B. Angular distribution

The J^P assignment for the observed structure is investigated by examining the distribution of $|\cos\theta|$, where θ is the η polar angle in the J/ψ rest frame. If $J^P = 1^-$, the decay of $J/\psi \rightarrow \eta X$ takes place through a P wave, neglecting the higher orbital angular momenta due to the closeness of the threshold, and the $|\cos\theta|$ is expected to follow $1 + \cos^2\theta$ distribution. If $J^P = 1^+$, the above decay takes place through an S wave, and the $|\cos\theta|$ distribution is expected to be flat.

The data is divided into four intervals of $|\cos\theta|$, and the total signal yield in each interval is obtained with the same method of simultaneous fit with 1^+ assumption as described above. After efficiency correction and normalization, the $|\cos\theta|$ distribution of data is shown in Fig. 6, together with the fitting results with the 1^- and 1^+ assumptions. The 1^- assumption determines that the

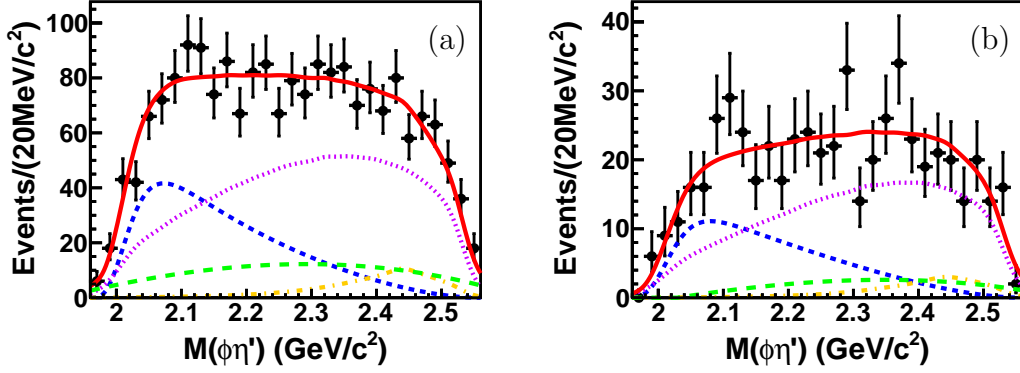


FIG. 4. Results of the simultaneous fit with the 1^- assumption for modes I (a) and II (b). The crosses are experimental data and the solid curves show the fit model. The dashed curves are the signal component. The dotted curves show the background from the $J/\psi \rightarrow \phi\eta\eta'$ PHSP process. The pecked curves represent the background from the $J/\psi \rightarrow \phi f_0(1500), f_0(1500) \rightarrow \eta\eta'$ process. The long-dashed curves show the non- ϕ and/or non- η' backgrounds.

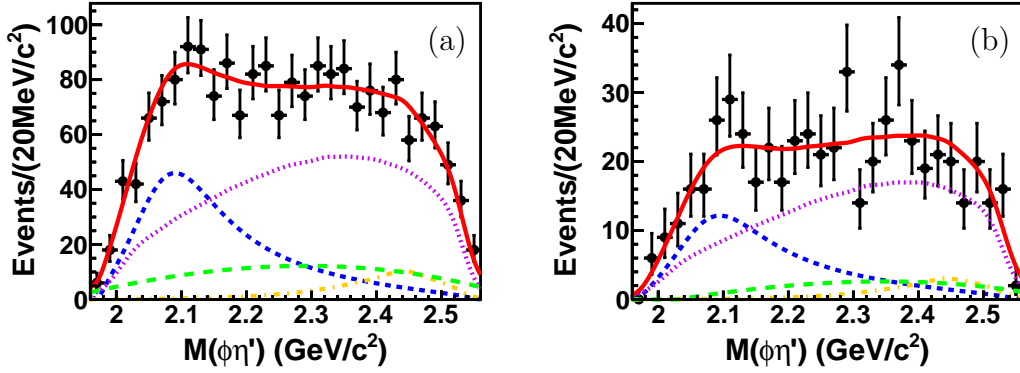


FIG. 5. Results of the simultaneous fit with the 1^+ assumption for modes I (a) and II (b). The crosses are experimental data and the solid curves show the fit model. The dashed curves are the signal component. The dotted curves show the background from the $J/\psi \rightarrow \phi\eta\eta'$ PHSP process. The pecked curves represent the background from the $J/\psi \rightarrow \phi f_0(1500), f_0(1500) \rightarrow \eta\eta'$ process. The long-dashed curves show the non- ϕ and/or non- η' backgrounds.

$\chi^2/\text{d.o.f.}$ value is $10.55/3 = 3.52$ and the 1^+ assumption determines that the value is $4.41/3 = 1.47$. Although the $\chi^2/\text{d.o.f.}$ value favors the 1^+ assumption, hardly could these two assumptions be distinguished due to the limited statistics. The 0^+ assumption is ruled out for it violates the law of J^P conservation, and the 0^- assumption could be rejected at 99.5% confidence level from the Pearson χ^2 test. The results of simultaneous fit with 1^- assumption are consistent with those from 1^+ .

C. Measurement of product branching fraction

The product branching fraction of $\eta\phi\eta'$ final state through the observed structure is calculated by

$$\mathcal{B}(J/\psi \rightarrow \eta X) \times \mathcal{B}(X \rightarrow \phi\eta') = \frac{N_{\text{sig}}}{N_{J/\psi} \mathcal{B}(\eta \rightarrow 2\gamma) \mathcal{B}(\phi \rightarrow K^+ K^-) \bar{\epsilon}} \quad (3)$$

where N_{sig} is the total signal yield from the two modes in the simultaneous fit; $\bar{\epsilon}$ is $\mathcal{B}(\eta' \rightarrow \gamma\pi^+\pi^-)\epsilon_{\text{I}} + \mathcal{B}(\eta' \rightarrow \eta\pi^+\pi^-)\mathcal{B}(\eta \rightarrow 2\gamma)\epsilon_{\text{II}}$, where ϵ_{I} and ϵ_{II} are the detection efficiencies determined from signal MC simulation after considering the J^P value of the structure and the angular distributions of the η , ϕ and η' particles; other variables have been defined before. The measured N_{sig} and $\mathcal{B}(J/\psi \rightarrow \eta X) \times \mathcal{B}(X \rightarrow \phi\eta')$ with 1^- and 1^+ assumptions are summarized in Table II, where the uncertainties are statistical only.

TABLE II. Measured N_{sig} and $\mathcal{B}(J/\psi \rightarrow \eta X) \times \mathcal{B}(X \rightarrow \phi\eta')$ with 1^- and 1^+ assumptions.

J^P	N_{sig}	$\mathcal{B}(J/\psi \rightarrow \eta X) \times \mathcal{B}(X \rightarrow \phi\eta')$
1^-	658 ± 77	$(9.8 \pm 1.2) \times 10^{-5}$
1^+	642 ± 88	$(9.6 \pm 1.4) \times 10^{-5}$

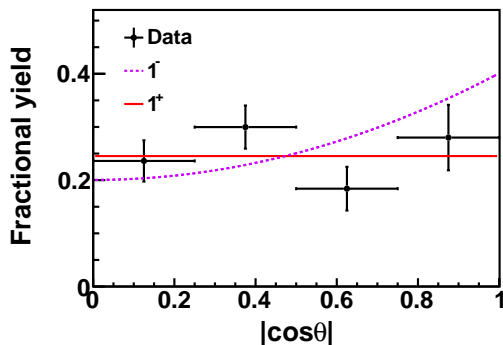


FIG. 6. Distribution of η polar angle in the J/ψ rest frame. The crosses are experimental data. The dashed curve is the fitting result with the 1^- assumption, and the solid curve is that with the 1^+ assumption.

D. Systematic uncertainties

Table III and Table IV summarise the systematic uncertainties in the measurements of mass and width of the observed structure, as well as $\mathcal{B}(J/\psi \rightarrow \eta X) \times \mathcal{B}(X \rightarrow \phi \eta')$ with 1^- and 1^+ assumptions, respectively. In case there are differences between the uncertainties from two modes, the more conservative values are used.

TABLE III. Systematic uncertainties in the mass and width of the observed structure, as well as $\mathcal{B}(J/\psi \rightarrow \eta X) \times \mathcal{B}(X \rightarrow \phi \eta')$ (denoted as \mathcal{B}_X in this table) with the 1^- assumption.

Sources	Mass(MeV/ c^2)	Width(MeV)	$\mathcal{B}_X(\%)$
Signal parametrization	9.1	2	2.9
$f_0(1500)$	9.5	5	11.6
Sideband regions	0.9	2	0.4
Fitting range	6.3	3	3.1
$M(\pi^+\pi^-)$ requirement	1.8	2	0
Extra structures	2.5	0	1.1
Momentum calibration	0.7	-	-
MDC tracking	-	-	4.0
PID	-	-	4.0
Photon detection	-	-	2.4
Kinematic fit	-	-	3.0
Mass window for η	-	-	0.7
Mass window for ϕ	-	-	1.0
Mass window for η'	-	-	0.7
MC statistics	-	-	0.9
Branching fractions	-	-	2.1
Number of J/ψ	-	-	0.6
Total	15.0	7	14.5

The signal parametrization is changed from a constant-width BW function to a BW function with mass-dependent width. The impact on the signal yield is taken as the uncertainty of $\mathcal{B}(J/\psi \rightarrow \eta X) \times \mathcal{B}(X \rightarrow \phi \eta')$. The pole mass (m_{pole}) and pole width (Γ_{pole}) are obtained by solving for the complex equation $P = m_{\text{pole}} - i\Gamma_{\text{pole}}/2$ for which the BW denominator is zero, and the differences between the mass and width from nominal fit and m_{pole}

TABLE IV. Systematic uncertainties in the mass and width of the observed structure, as well as $\mathcal{B}(J/\psi \rightarrow \eta X) \times \mathcal{B}(X \rightarrow \phi \eta')$ (denoted as \mathcal{B}_X in this table) with the 1^+ assumption.

Sources	Mass(MeV/ c^2)	Width(MeV)	$\mathcal{B}_X(\%)$
Signal parametrization	2.4	0	0.4
$f_0(1500)$	2.6	19	13.4
Sideband regions	0.7	1	0.4
Fitting range	1.1	6	3.2
$M(\pi^+\pi^-)$ requirement	1.3	1	0
Extra structures	0.7	1	1.9
Momentum calibration	0.7	-	-
MDC tracking	-	-	4.0
PID	-	-	4.0
Photon detection	-	-	2.4
Kinematic fit	-	-	2.3
Mass window for η	-	-	0.7
Mass window for ϕ	-	-	1.0
Mass window for η'	-	-	0.7
MC statistics	-	-	0.9
Branching fractions	-	-	2.1
Number of J/ψ	-	-	0.6
Total	4.2	20	15.7

and Γ_{pole} are considered as the uncertainties of mass and width, respectively. To obtain the uncertainties associated with the $f_0(1500)$ component of the data, the levels of the background that are included in the simultaneous fit are varied by 1σ [9, 11], where σ denotes the uncertainty on the determined number of the $f_0(1500)$, and the maximum changes in the fit results are regarded as uncertainties. The sideband regions of ϕ and η' mesons are varied by 1σ (the width of signal region corresponds to 3σ), and the effects on the results of the simultaneous fit are assigned as uncertainties. We vary the range of the simultaneous fit by 5% and take the largest deviations of the fitting results as uncertainties. To obtain the uncertainties due to the $M(\pi^+\pi^-)$ requirement for mode I, it is relaxed from 0.87 to 0.90 GeV/ c^2 and the effects on the fitting results are considered as uncertainties. The two possible extra structures around 2.3 GeV/ c^2 in Figs. 4 (b) and 5 (b) are considered. Following the same procedure in Ref. [13], we use a BW function convolved with a resolution function to describe them and the corresponding significances are determined to be less than 1.1σ . In that case, they are not considered in the nominal result. However, their impacts on the fitting results are taken as systematic uncertainties. The difference between the fitted η mass and that from PDG [11] is taken as uncertainty due to momentum calibration. The descriptions of other items could refer to Table I. The total systematic uncertainties are obtained by summing all individual contributions in quadrature, assuming they are independent.

VI. SUMMARY AND DISCUSSION

In summary, using $(1310.6 \pm 7.0) \times 10^6$ J/ψ events collected with the BESIII detector, we report the observation and study of the $J/\psi \rightarrow \phi\eta\eta'$ process. Its branching fraction including all possible intermediate states is determined to be $(2.32 \pm 0.06 \pm 0.16) \times 10^{-4}$. A structure denoted as X is observed in the $\phi\eta'$ mass spectra in two dominant η' decay modes, and a simultaneous fit is performed. Assuming the J^P value of the structure as 1^- , the significance of the structure is evaluated to be 5.3σ ; the mass and width are determined to be $(2002.1 \pm 27.5 \pm 15.0)$ MeV/ c^2 and $(129 \pm 17 \pm 7)$ MeV, respectively; the product branching fraction $\mathcal{B}(J/\psi \rightarrow \eta X) \times \mathcal{B}(X \rightarrow \phi\eta')$ is measured to be $(9.8 \pm 1.2 \pm 1.5) \times 10^{-5}$; the mass of the observed structure is almost 6σ away from that of the $Y(2175)$ in PDG [11], suggesting the structure might not be the $Y(2175)$. Assuming the J^P value of the structure as 1^+ , the significance of the structure is evaluated to be 4.9σ ; the mass and width are determined to be $(2062.8 \pm 13.1 \pm 4.2)$ MeV/ c^2 and $(177 \pm 36 \pm 20)$ MeV, respectively; the product branching fraction $\mathcal{B}(J/\psi \rightarrow \eta X) \times \mathcal{B}(X \rightarrow \phi\eta')$ is measured to be $(9.6 \pm 1.4 \pm 1.6) \times 10^{-5}$. The angular distribution is studied and the 1^- and 1^+ assumptions could hardly be distinguished due to the limited statistics. No candidates in PDG have compatible mass, width and J^P values with the new structure. More studies with the larger J/ψ data sample in the future might help to better understand the observed structure, among which the J^P determination and precise measurements of the mass, width, and

product branching fraction are especially important.

ACKNOWLEDGMENTS

The BESIII collaboration thanks the staff of BEPCII and the IHEP computing center for their strong support. This work is supported in part by National Key Basic Research Program of China under Contract No. 2015CB856700; National Natural Science Foundation of China (NSFC) under Contracts Nos. 11335008, 11425524, 11625523, 11635010, 11735014; the Chinese Academy of Sciences (CAS) Large-Scale Scientific Facility Program; the CAS Center for Excellence in Particle Physics (CCEPP); Joint Large-Scale Scientific Facility Funds of the NSFC and CAS under Contracts Nos. U1532257, U1532258; CAS Key Research Program of Frontier Sciences under Contracts Nos. QYZDJ-SSW-SLH003, QYZDJ-SSW-SLH040; 100 Talents Program of CAS; INPAC and Shanghai Key Laboratory for Particle Physics and Cosmology; German Research Foundation DFG under Contracts Nos. Collaborative Research Center CRC 1044, FOR 2359; Istituto Nazionale di Fisica Nucleare, Italy; Koninklijke Nederlandse Akademie van Wetenschappen (KNAW) under Contract No. 530-4CDP03; Ministry of Development of Turkey under Contract No. DPT2006K-120470; National Science and Technology fund; The Swedish Research Council; U. S. Department of Energy under Contracts Nos. DE-FG02-05ER41374, DE-SC-0010118, DE-SC-0010504, DE-SC-0012069; University of Groningen (RuG) and the Helmholtzzentrum fuer Schwerionenforschung GmbH (GSI) Darmstadt; Institute for Basic Science (Korea) under project code IBS-R016-D1.

-
- [1] D. Morgan and M. R. Pennington, Phys. Rev. D **48**, 5422 (1993).
 - [2] U. G. Meissner and J. A. Oller, Nucl. Phys. **A679**, 671 (2001); L. Roca, J. E. Palomar, E. Oset, and H. C. Chiang, *ibid.* **A744**, 127 (2004); T. A. Lahde and U. G. Meissner, Phys. Rev. D **74**, 034021 (2006).
 - [3] B. Liu, M. Buescher, F. K. Guo, C. Hanhart, and U. G. Meissner, Eur. Phys. J. C **63**, 93 (2009).
 - [4] P. Chatzis, A. Faessler, T. Gutsche, and V. E. Lyubovitskij, Phys. Rev. D **84**, 034027 (2011).
 - [5] L. Kopke, *Proceedings of the XXIIIrd International Conference on High Energy Physics, Berkeley, 1986*, edited by S. Loken (World Scientific, Singapore, 1987).
 - [6] A. Falvard *et al.* (DM2 Collaboration), Phys. Rev. D **38**, 2706 (1988).
 - [7] M. Ablikim *et al.* (BES Collaboration), Phys. Lett. B **598**, 149 (2004).
 - [8] M. Ablikim *et al.* (BES Collaboration), Phys. Lett. B **603**, 138 (2004).
 - [9] M. Ablikim *et al.* (BES Collaboration), Phys. Lett. B **607**, 243 (2005).
 - [10] M. Ablikim *et al.* (BES Collaboration), Phys. Lett. B **633**, 681 (2006).
 - [11] M. Tanabashi *et al.* (Particle Data Group), Phys. Rev. D **98**, 030001 (2018).
 - [12] M. Ablikim *et al.* (BES Collaboration), Phys. Rev. Lett. **100**, 102003 (2008).
 - [13] M. Ablikim *et al.* (BESIII Collaboration), Phys. Rev. D **91**, 052017 (2015).
 - [14] G. J. Ding and M. L. Yan, Phys. Lett. B **650**, 390 (2007).
 - [15] M. Ablikim *et al.* (BESIII Collaboration), Chin. Phys. C **41**, 013001 (2017).
 - [16] M. Ablikim *et al.* (BESIII Collaboration), Nucl. Instrum. Methods Phys. Res., Sect. A **614**, 345 (2010).
 - [17] C. H. Yu *et al.*, Proceedings of IPAC2016, Busan, Korea, 2016, doi:10.18429/JACoW-IPAC2016-TUYA01.
 - [18] S. Agostinelli *et al.* (GEANT4 Collaboration), Nucl. Instrum. Methods Phys. Res., Sect. A **506**, 250 (2003).
 - [19] S. Jadach, B. F. L. Ward, and Z. Was, Comput. Phys. Commun. **130**, 260 (2000); Phys. Rev. D **63**, 113009 (2001).
 - [20] D. J. Lange, Nucl. Instrum. Methods Phys. Res., Sect. A **462**, 152 (2001); R. G. Ping, Chin. Phys. C **32**, 599

- (2008).
- [21] J. C. Chen, G. S. Huang, X. R. Qi, D. H. Zhang, and Y. S. Zhu, Phys. Rev. D **62**, 034003 (2000); R. L. Yang, R. G. Ping and H. Chen, Chin. Phys. Lett. **31**, 061301 (2014).
- [22] E. Richter-Was, Phys. Lett. B **303**, 163 (1993).
- [23] M. Ablikim *et al.* (BESIII Collaboration), Phys. Rev. Lett. **107**, 182001 (2011).
- [24] M. Ablikim *et al.* (BESIII Collaboration), Phys. Rev. D **87**, 012007 (2013).
- [25] G. D'Agostini, Nucl. Instrum. Methods Phys. Res., Sect. A **346**, 306 (1994).
- [26] M. Ablikim *et al.* (BESIII Collaboration), Phys. Rev. Lett. **107**, 092001 (2011).
- [27] M. Ablikim *et al.* (BESIII Collaboration), Phys. Rev. D **83**, 112005 (2011).
- [28] M. Ablikim *et al.* (BESIII Collaboration), Phys. Rev. D **96**, 112012 (2017).
- [29] M. Ablikim *et al.* (BESIII Collaboration), Phys. Rev. D **87**, 012002 (2013).